Dalton Transactions

Cite this: *Dalton Trans.*, 2012, **41**, 10854

www.rsc.org/dalton

PAPER

Novel Pd(II)–salen complexes showing high *in vitro* anti-proliferative effects against human hepatoma cancer by modulating specific regulatory genes†

Mohammad Azam,*[a] Zahid Hussain,[b] Ismail Warad,[a] Saud I. Al-Resayes,[a] Mohd. Shahnawaz Khan,[c] Mohammad Shakir,[d] Agata Trzesowska-Kruszynska[e] and Rafal Kruszynski[e]

Received 27th May 2012, Accepted 28th June 2012
DOI: 10.1039/c2dt31143g

We have reported the synthesis of a novel salen ligand and its mononuclear Pd–salen complexes derived from 2-{[2-hydroxy-3-{[(*E*)-(2-hydroxyphenyl)methylidene]amino}propyl)imino]methyl}phenol. The newly synthesized and isolated Pd(II) complexes have been identified and fully characterized by various physico-chemical studies *viz*., elemental analyses, IR, UV-Vis, ^{1}H, ^{13}C NMR spectroscopy, electron spray ionization mass spectrometry (ESI-MS) and TGA/DTA studies. The molecular structure of the salen ligand has been ascertained by single-crystal XRD and it is coordinated to Pd(II) ion through two nitrogen and two oxygen atoms. The UV-Vis data clearly suggest a square-planar environment around both the Pd(II) ions. The DNA binding studies of the synthesized compounds has been investigated by electron spectroscopy and fluorescence measurements. The results suggest that Pd(II) complexes bind to DNA strongly as compared to the free ligand. The free salen ligand and its Pd(II) complexes have also been tested against human hepatoma cancer cell line (Huh7) and results manifested exceptional anti-proliferative effects of the Pd(II) complexes. The anti-proliferative activity of Pd(II) complexes has been modulated by specific regulatory genes.

1. Introduction

Since the revolutionary discovery of cisplatin, *cis*-(diammine-dichloroplatinum(II), as an anticancer drug by Rosenberg, extensive research work has been carried out on platinum-based chemotherapeutic compounds.[1,2] Despite its remarkable success with high efficacy against human testicular, ovarian, bladder, head and neck carcinomas, several side effects such as limited water solubility and the dose-dependent toxicities, mainly nephrotoxicity, neurotoxicity, cytotoxicity and emetogensis are the major drawbacks associated with this drug.[3–5] Besides this, prolonged use of cisplatin also leads to cellular resistance in some of the most common cancers.[6] Therefore, to overcome these problems, attempts are being made to replace this drug with suitable alternatives, and numerous transition-metal complexes have been synthesized and screened for their anti-cancer activities.[6] The first non-platinum complex tested in clinical trials was *cis*-[$(CH_3CH_2O)_2$(bzac)$_2$Ti(IV)] used against a wide variety of ascites and solid tumors.[7–8] The significant similarity between the coordination chemistry of Pd(II) and Pt(II) compounds has advocated studies of Pd(II) complexes as antitumor drugs, but the higher lability in ligand exchange at the Pd centre (10^5-fold *vs.* Pt) may cause rapid hydrolysis processes leading to dissociation of complex and formation of very reactive species unable to reach their pharmacological targets.[9] These problems could be overcome by using the bulky heterocyclic and chelating ligands. A number of palladium complexes with aromatic *N*- and *N*,*N*-containing ligands have shown very promising antitumor characteristics.[10,11] Recent studies demonstrate that some Pd(II) complexes exhibit a noticeable *in vitro* cytotoxic activity, comparable to standard platinum-based drugs, cisplatin, carboplatin and oxaliplatin.[12] Over the years chemists have prepared ligands with a wide range of features designed to achieve their particular targets. In this context, the chemistry of metal complexes containing salen-type ligands has received substantial attention because of their versatility and wide range of complexing ability, and are also the key points in the development of inorganic biochemistry, catalysis, magnetism, medical imaging *etc.*[13–16] Some of the salen complexes have also revealed interesting antioxidant and antitumor properties.[17] Here, we report the synthesis and characterization of a novel salen ligand derived from 1,3-diaminopropanol and *o*-hydroxybenzaldehyde and its Pd(II) complexes. The synthesized ligand and its complexes have been screened for their *in vitro* viability and anti-proliferative activities in

[a]*Department of Chemistry, King Saud University, P. O. Box 2455, Riyadh 11451, KSA. E-mail: azam_res@yahoo.com; Tel: +966-596441517*
[b]*Center of Excellence in Biotechnology Research, King Saud University, Riyadh, 11451, KSA*
[c]*PRC, Department of Biochemistry, King Saud University, Riyadh 11451, KSA*
[d]*Department of Chemistry, Aligarh Muslim University, Aligarh 202002, India*
[e]*Department of X-ray Crystallography and Crystal Chemistry, Institute of General and Ecological Chemistry, Technical University of Lodz, Zeromskiego 116, 90-924, Lodz, Poland*

†Electronic supplementary information (ESI) available. CCDC 876116. For ESI and crystallographic data in CIF or other electronic format see DOI: 10.1039/c2dt31143g

human hepatocellular carcinoma (Huh7) cells. We have also analyzed the effect of the salen ligand and its Pd(II) complexes on the expression of the key genes involved in tumor promoting and tumor suppressing function such as Wnt-1, Urokinase plasminogen activator (uPA), Ras association domain family 1A (RASSF1A) and transforming growth factor-β (TGF-β).

2. Experimental

2.1 Materials and methods

All the reagents and solvents used were of analAR grade quality and were purchased from Merck and used as received. All complexations reactions were carried out using standard Schlenk techniques under argon. Elemental analyses were recorded on Elementar Varrio EL analyzer. FT-IR (4000–400 cm^{-1}) spectra were obtained as KBr pellets using a Perkin Elmer 621 spectrophotometer. ^{1}H and ^{13}C NMR spectra of ligand and its Pd(II) complexes were recorded in $CDCl_3$ using a JEOL 400 spectrometer. Chemical shifts are quoted in parts per million from TMS. Mass spectrometry was performed with a Micromass Quattro Premier tandem MS fitted with an ESI interface and controlled by MassLynx 4.1 software. MS/MS detection was performed with electrospray positive ionization mode. Electronic spectra of the complexes were obtained in dichloromethane on a Pharmacia LKB-Biochem UV-vis spectrophotometer at room temperature. Thermal behavior of the synthesized compounds was studied by using SDTQ-600 (TA Instrument) in a helium atmosphere (100 ml min^{-1}) at a heating rate of 20 °C min^{-1}, in the temperature range from ambient to 800 °C.

2.2 Synthesis

2.2.1 Synthesis of salen ligand L. A methanolic solution of *o*-hydroxybenzaldehyde (2 mmol) was added dropwise to a methanolic solution of 1,3-diaminopropanol (1 mmol). The reaction mixture was stirred for 5 h resulting in a clear yellow solution. The resulting solution was concentrated to 1 ml followed by addition of 20 ml of diethyl ether to cause precipitation. The precipitate was removed by filtration and after couple of days yellow crystals suitable for X-ray diffraction appeared in the filtrate. The crystals were filtered off, washed with hexane and dried *in vacuo*.

Yield 70%, color: yellow, mp 138 °C; molecular formula $C_{17}H_{18}N_2O_3$; ^{1}H NMR ($CDCl_3$): δ (ppm) 13.82 (Ar–OH), 8.35 (s, –CH═N), 6.79–7.10 (m, Ar–H), 3.58–3.65 (m, 4H $–CH_2$), 3.65 (s, 1H, –CH). ^{13}C NMR ($CDCl_3$): δ (ppm) 163.68 (–CH═N), 62.85 ($–CH_2$), 69.15 (–CH), 160.15, 131.85, 131.91, 116.45, 118.50 and 117.21 (aromatic carbons), Anal. Calc.: C, 68.44; H, 6.08; N, 9.39; O, 16.08%. Found: C, 68.25; H, 5.97; N, 9.28; O, 15.98%. IR, ν/cm^{-1}: 3270 ($\nu_{Ph–OH}$), 1655 ($\nu_{–CH=N}$), 1278 ($\nu_{C–O\ phenolic}$).

2.2.2 Synthesis of complexes $[PdLCl_2]$ 1 and $[PdL(OAc)_2]$ 2. A solution of Pd(II) salt $PdCl_2$ or $Pd(OAc)_2$ (0.50 mmol) dissolved in 10 ml CH_2Cl_2 was added dropwise to 10 ml CH_2Cl_2 solution of ligand (0.50 mmol). The resultant reaction mixture was stirred for 30 min resulting in a clear yellow solution. The resulting solution was concentrated to 1 ml followed by addition of 10 ml of hexane for precipitation. The resulting colored precipitate was isolated and recrystallised from dichloromethane–hexane and obtained in analytically pure form. No crystals was found to be suitable for single-crystal XRD.

1: Yield 70%, color: yellow, mp 138 °C; molecular formula $C_{17}H_{18}N_2O_3PdCl_2$; ^{1}H NMR ($CDCl_3$): δ (ppm) 8.41 (s, –CH═N), 6.89–6.97 (m, Ar–H), 3.87 (s, 1H, –CH), 3.86–3.72 (m, 4H $–CH_2$). ^{13}C NMR ($CDCl_3$): δ (ppm) 167.56 (–CH═N), 63.36 ($–CH_2$), 70.58 (–CH), 161.03, 132.71, 131.68, 118.92, 118.72 and 117.07 (aromatic carbons), Anal. Calc.: C, 42.93; H, 3.81; N, 5.89; O, 10.09; Pd, 22.37; Cl, 14.91%. Found: C, 42.88; H, 3.79; N, 5.85; O, 9.98; Pd, 22.32; Cl, 14.85%. IR, ν/cm^{-1}: 1290 ($\nu_{Pd–O}$), 1625 ($\nu_{–CH=N}$).

2: Yield 70%, color: yellow, mp 138 °C; molecular formula $C_{21}H_{24}N_2O_7Pd$; ^{1}H NMR ($CDCl_3$): δ (ppm) 8.56 (s, –CH═N), 6.87–7.97 (m, Ar–H), 5.23 (s, 1H, –CH), 3.61–3.75 (m, 4H $–CH_2$), ^{13}C NMR ($CDCl_3$): δ (ppm) 172.25 (–CH═N), 63.85 ($–CH_2$), 70.15 (–CH), 167.85, 161.80, 132.15, 132.25, 117.75, 118.23 (aromatic carbons), Anal. Calc: C, 48.24; H, 4.62; N, 5.35; O, 21.42; Pd, 20.35%. Found: C, 48.19; H, 4.57; N, 5.31; O, 21.37; Pd, 20.28%. IR, ν/cm^{-1}: 1282 ($\nu_{Pd–O}$), 1648 ($\nu_{–CH=N}$).

2.3 Crystal structure determination

The yellow prism crystal of free ligand **L** was sealed in glass capillary filled with helium and then mounted on a KM-4-CCD automatic diffractometer equipped with CCD detector, and used for data collection. X-Ray intensity data were collected with graphite-monochromated Cu-Kα (λ = 1.54178 Å) radiation at 291.0(3) K, with ω scan mode. A 34 s exposure time was used and reflections inside the Ewald sphere were collected up to θ = 68.04°. The unit cell parameters were determined from the 3008 strongest reflections. Details concerning crystal data and refinement are given in Table 1. Examination of reflections on two reference frames monitored after each 20 frames measured showed no loss of the intensity during measurement. During the data reduction Lorentz, polarization and numerical absorption corrections were applied.[18] The structure was solved by partial structure expansion procedure. All the non-hydrogen atoms were refined anisotropically using full-matrix, least-squares technique on F^2. All the hydrogen atoms were found from difference Fourier synthesis after four cycles of anisotropic refinement, and refined as "riding" on the adjacent atom with geometric idealisation after each cycle of refinement and individual isotropic displacement factors equal to 1.2 times the value of the equivalent displacement factor of the parent carbon atoms and 1.5 times of the parent oxygen atoms. The hydroxyl groups were allowed to rotate about the O–C bond axes. The studied crystal was racemically twinned with 0.56 : 0.44 participation of chiral domains. The Flack parameter was refined as a full matrix parameter. SHELXS97, SHELXL97 and SHELXTL programs were used for all the calculations.[19] Atomic scattering factors were those incorporated in the computer programs. Selected interatomic bond distances and angles are listed in Table 2 and intermolecular interactions are listed in Table 3.

2.4 DNA binding assays of free ligand L and complexes 1 and 2

DNA binding experiments were performed utilizing UV-Vis and fluorescence spectroscopy. The purity of calf thymus DNA was confirmed by taking the ratio of the absorbance values at 260 and 280 nm in tris-EDTA (10 mM, pH 7.0) buffer, which was found to be 1.8 : 1, indicating that the DNA was sufficiently free of protein and other contaminants. The concentration of DNA for binding studies was determined by absorption spectroscopy at 260 nm using the molar extinction coefficient value of 6600 $dm^3\ mol^{-1}\ cm^{-1}$. For measurements free ligand **L** and its complexes **1** and **2** were dissolved in 5% DMSO. Absorption titration experiments were performed with a fixed concentration of DNA (0.1 mM) while gradually increasing concentration of the free ligand **L** and its complexes **1** and **2** from 10 to 50 μM.

To further characterize the ligand–DNA binding interactions fluorescence quenching experiments were performed. Nucleic acid binding assays of synthesized compounds were carried out in the presence of ethidium bromide. DNA and ethidium bromide (EB) were dissolved in tris-EDTA (10 mM, pH 7.0) buffer at concentrations of 4 and 1 μg ml^{-1}, respectively. The concentration of ligand **L** and complexes **1** and **2** was 50 μM. To perform the experiments, DNA was pretreated with ethidium bromide for 30 min. Then the test solutions were added to this mixture of EB–DNA, and the change in the fluorescence intensity was measured. Fluorescence measurements were carried out on a Shimadzu spectrofluorimeter model RF-540 equipped with a data-recorder DR-3. The fluorescence was recorded at 485–685 nm after exciting the solution at 478 nm. The slits were set at 5 nm for excitation and emission. The path length of the sample was 1 cm.

Table 1 Crystal and structure refinement data of compound **1**

Compound	**1**
Empirical formula	$C_{17}H_{18}N_2O_3$
M_r	298.33
Crystal system	Monoclinic
Space group	*Cc* (no. 9)
a/Å	35.6816(19)
b/Å	11.2773(4)
c/Å	16.3321(9)
β/°	109.142(4)
V/Å^3	6208.5(5)
Z, D_c/Mg m^{-3}	16, 1.277
μ/mm^{-1}	0.721
F(000)	2528
Crystal size/mm	0.066 × 0.061 × 0.060
θ range for data collection/°	2.62–68.04
Index ranges, *hkl*	−42 to 42, −10 to 13, −19 to 19
Reflections collected/unique	35541/10801
R_{int}	0.0256
Completeness (%)	99.3 (to $\theta = 67°$)
Min., max. transmission	0.948, 0.963
Data/restraints/parameters	10801/2[a]/806
Goodness-of-fit on F^2	1.021
Final *R* indices [$I > 2\sigma(I)$]	$R_1 = 0.0369$, w$R_2 = 0.1067$
R indices (all data)	$R_1 = 0.0383$, w$R_2 = 0.1092$
$\Delta\rho_{max,\ min}$/e Å^{-3}	0.227, −0.172

[a] Floating origin restraints.

Table 3 Hydrogen bond geometries of compound **1** [Å, °][a]

D–H···A	*d*(D–H)	*d*(H···A)	*d*(D···A)	∠(DHA)
O1–H1–N1	0.82	1.89	2.601(2)	145.1
O2–H2–O21^{i}	0.82	2.39	2.921(2)	123.7
O3–H3A–N2	0.82	1.89	2.610(2)	146.9
O21–H21–N21	0.82	1.85	2.578(2)	148.0
O22–H22–O62^{ii}	0.89	2.20	2.976(2)	145.4
O23–H23A–N22	0.82	1.85	2.577(2)	147.7
O41–H41–N41	0.82	1.89	2.598(2)	144.5
O42–H42–O22	0.82	2.04	2.851(2)	171.3
O43–H43A–N42	0.82	1.86	2.587(2)	147.5
O61–H61–N61	0.82	1.86	2.587(2)	146.3
O62–H62–O2^{iii}	0.82	2.03	2.837(2)	166.5
O63–H63A–N62	0.82	1.87	2.599(2)	147.6
C25–H25–O1^{iv}	0.93	2.57	3.215(3)	126.4
C50–H50B–N41	0.97	2.62	2.978(3)	102.3
C68–H68A–N62	0.97	2.60	2.954(3)	101.7

[a] Symmetry transformations used to generate equivalent atoms: (i) *x*, −*y* + 1, *z* + 1/2; (ii) *x* − 1/2, *y* − 1/2, *z*; (iii) *x* + 1/2, −*y* + 3/2, *z* − 1/2; (iv) *x*, *y*, *z* − 1.

Table 2 Selected structural data of compound **1** [Å, °]

C2–O1	1.332(2)	C22–O21	1.325(2)	C42–O41	1.343(3)	C62–O61	1.341(2)
C7–N1	1.266(2)	C27–N21	1.257(2)	C47–N41	1.276(2)	C67–N61	1.269(2)
N1–C8	1.447(2)	N21–C28	1.465(2)	N41–C48	1.456(2)	N61–C68	1.455(2)
C9–O2	1.409(2)	C29–O22	1.405(2)	C49–O42	1.411(2)	C69–O62	1.418(2)
C10–N2	1.459(2)	C30–N22	1.454(2)	C50–N42	1.453(2)	C70–N62	1.448(2)
N2–C11	1.265(2)	N22–C31	1.260(2)	C51–N42	1.260(3)	N62–C71	1.269(2)
C13–O3	1.340(2)	C33–O23	1.345(3)	C53–O43	1.344(2)	C73–O63	1.348(3)
C7–N1–C8	119.8(2)	C27–N21–C28	119.7(2)	C47–N41–C48	117.8(2)	C67–N61–C68	119.8(2)
C11–N2–C10	119.1(2)	C31–N22–C30	119.6(2)	C51–N42–C50	119.6(2)	C71–N62–C70	119.0(2)
C2–C1–C7–N1	−1.8(3)	C22–C21–C27–N21	−0.6(3)	C42–C41–C47–N41	1.9(3)	C62–C61–C67–N61	−0.5(3)
C1–C7–N1–C8	178.3(2)	C21–C27–N21–C28	177.2(2)	C41–C47–N41–C48	179.3(2)	C61–C67–N61–C68	179.7(2)
C7–N1–C8–C9	128.3(2)	C27–N21–C28–C29	171.9(2)	C47–N41–C48–C49	−124.7(2)	C67–N61–C68–C69	−103.2(2)
N1–C8–C9–C10	169.4(2)	N21–C28–C29–C30	−175.8(2)	N41–C48–C49–C50	−63.3(2)	N61–C68–C69–C70	−176.7(2)
C8–C9–C10–N2	−174.7(2)	C28–C29–C30–N22	171.5(2)	C48–C49–C50–N42	175.9(2)	C68–C69–C70–N62	59.9(2)
C9–C10–N2–C11	−175.6(2)	C29–C30–N22–C31	123.4(2)	C49–C50–N42–C51	103.8(2)	C69–C70–N62–C71	127.4(2)
C10–N2–C11–C12	177.9(2)	C30–N22–C31–C32	−179.5(2)	C50–N42–C51–C52	−178.9(2)	C70–N62–C71–C72	−178.2(2)
N2–C11–C12–C13	−2.7(3)	N22–C31–C32–C33	0.4(3)	N42–C51–C52–C53	1.4(3)	N62–C71–C72–C73	−0.3(3)

To determine the DNA-binding ability of free ligand **L** and complexes **1** and **2**, fluorescence intensity data were analyzed by the Stern–Volmer equation:[20]

$$F_0/F = 1 + K_{sv}[Q]$$

where, F and F_0 are the fluorescence intensity with and without the quencher (complex–DNA), K_{sv} is the Stern–Volmer quenching constant, and [Q] is the concentration of the quencher. The K_{SV} value of the complexes [EB + DNA + **L**], [EB + DNA + **1**] and [EB + DNA + **2**] were calculated to be 1.23×10^5, 3.85×10^5 and 3.67×10^5 M^{-1}, respectively. A higher K_{SV} value of complex **1** suggests its stronger quenching ability than complex **2** and free ligand **L**.

2.5 Cell culture and treatment

Human hepatoma cell line Huh7, was grown in Dulbecco's modified Eagle's medium (DMEM, Gibco-BRL) supplemented with 10% fetal bovine serum (FBS, Gibco-BRL) and 10 μg ml^{-1} gentamycin at 37 °C in 5% CO_2. In the treatment group, Huh7 cells were treated for 48 h with different test compounds (free ligand **L** or complexes **1** and **2** at final concentration of 0.1 μM), along with vehicle control alone (DMSO).

2.6 Cell proliferation assay

Huh7 cells were plated in quadruplicate at a density of 60 000 cells per well in 2 ml of respective culture media in six well plates. Cells were grown in the regular medium with 5% FBS in the control and treatment (free ligand **L**, complexes **1** and **2**) groups. Cell growth curves were analyzed at a dose of 0.1 μM. Cells were trypsinized, and the number of viable cells was determined by 0.4% Trypan Blue and counted at different time points starting from day 0 to 48 h, using a Coulter Counter (Model ZF; Coulter Electronics, Hertfordshire, UK).

2.7 Quantitative real-time RT-PCR of genes involved in cancer

Total cellular RNA from control and treated (free ligand **L**, complexes **1** and **2**) Huh7 cells were extracted using Trizol (Invitrogen Life Technologies) according to the manufacturer's protocol. 2 μg of total RNA was used for reverse transcription for cDNA preparation. The cDNA was then used for quantitation of genes involved in cancer by real time PCR (Applied Biosystem, 7500 Real Time PCR system). The primers used to quantify the different genes are listed in Table 4.

Table 4 Primer sequence and annealing temperatures (T_{anneal}) used for real-time PCR

Primer	Primer sequence	T_{anneal}/°C
Wnt-1	ACTCTCAGGACATGCTGGCT ACGAGGTCATTTTTCGTTGG	59
RASSF1A	ACCTCTGTGGCGACTTCATCT AGGTGAACTTGCAATGCGC	60
uPA	TTGCTCACCACAACGACATT GGCAGGCAGATGGTCTGTAT	56
TGF-β	CAAGGACCTCGGCTGGAA CCGGGTTATGCTGGTTGTACA	58
GAPDH	CGACCACTTTGTCAAGCTCA AGGGGTCTACATGGCAACTG	55–60

2.8 Statistical analysis

Results were analyzed as the mean ± SEM, and comparisons of the experimental data were by a two-tailed independent sample student's *t*-test. P values of <0.05 were considered statistically significant.

3. Results and discussions

The free salen ligand **L** has been synthesized by the interaction of *o*-hydroxybenzaldehyde with 1,3-diaminopropanol in 2 : 1 molar ratio in methanolic medium (Scheme 1). Pd(II) complexes, synthesized by reaction of free ligand **L** and Pd(II) salts in 1 : 1 molar ratio in dichloromethane in a Schlenck line under argon atmosphere, are colored microcrystalline solids. All the synthesized compounds are insoluble in water and soluble in all organic solvents. The formation of the free ligand and its Pd(II) complexes were confirmed on the basis of results of elemental analyses, molecular ion peak in ESI-MS spectra, characteristic absorption bands in FT-IR, and resonance signals in the ^1H and ^{13}C NMR spectra, and single-crystal XRD in the case of free ligand. The geometry around Pd(II) ions in the complexes was confirmed from the positions of absorption bands observed in UV-Vis spectra. The *in vitro* cytotoxic activity of the isolated free ligand **L** and its Pd(II) complexes have been tested against human Hepatoma Cancer Cell line, Huh7. Results suggest that Pd(II) complexes are more prominent in showing anti-proliferative activity when compared with the parent salen ligand.

3.1 X-Ray crystallography

A perspective view of free ligand **L** shows that all atoms occupy the same general positions (Fig. 1). The asymmetric part of the unit cell contains four molecules of free ligand **L**, and two of them (containing N41 and N61 atoms) are related by a non-crystallographic pseudosymmetry centre. In general, the molecules possess different conformations (Table 2), however for the

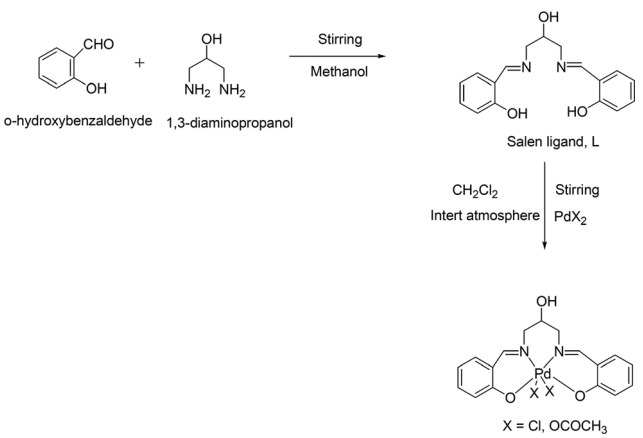

Scheme 1 Schematic representation of synthesis of salen ligand and its Pd(II) complexes.

molecules related by pseudosymmetry these differences are relatively small (Table 2). Some of the atoms of free ligand **L** molecules show differences in magnitude between components of the anisotropic displacement parameters along chemical bonds and in the equivalent isotropic displacement parameters in comparison to those of neighbouring bonded atoms. This originates primarily from the twisted character of parts of the studied molecules aliphatic chains (for details see torsion angles in Table 2) and thus less restricted atomic motion and static disorder in directions perpendicular to the interatomic bonds. The 2-hydroxybenzylideneaminomethyl moieties of all molecules of free ligand **L** are close to planarity, and while some obvious deviations of atoms from the respective weighted least squares planes exist, they are not larger than 0.04 Å. Mentioned moieties existing in duplicate within each molecule are inclined at 55.08(5), 62.15(5), 77.88(4) and 75.78(4)°, respectively for molecules containing N1, N21, N41, N61 atoms. The analysis of C–N bond lengths shows that the double bonds are fully localised within benzylideneamino moieties.

Each molecule of free ligand **L** contains two O–H···N intramolecular hydrogen bonds within 2-hydroxybenzylideneamino moieties (Table 3), each forming an S(6) motif. The molecules of **1** are connected by O–H···O intermolecular interactions (Table 3) to hydrogen-bonded tetramers, in which the hydroxyl substituents of the aliphatic part of the molecule act as hydrogen-bond donors, and hydroxyl substituents of aliphatic and aromatic parts act as hydrogen bond acceptors. The interactions form the N_1DDDD zero-dimensional unitary graph set, which is also zero-dimensional on higher graph set levels but it can be described as $N_3C_3^3(13)$ and $N_4C_3^3(13)D$. In the structure we observe two intramolecular C–H···N and one intermolecular C–H···O short contact (Table 3) which can be classified as weak hydrogen bonds.[21] This latter interaction expands the tetramers to hydrogen-bonded pillars extending along the crystallographic [001] axis. Stacking interactions are not observed within the crystal structure of free ligand **L** (the shortest distance between centroids of close to parallel aromatic rings is 4.8026 Å).

3.2 IR spectra

The most important IR bands and their assignments are listed in the Experimental section. When comparing the spectroscopic data of Pd(II) complexes with those of the free ligand, marked changes may be noticed in the ligand bands arising from various modes of donor groups involved in bonding to palladium ions (Fig. 2). The IR spectrum of the salen ligand exhibits a characteristic $\nu_{CH=N}$ stretching band at 1655 cm^{-1} which is shifted to lower frequency and appears at 1630 cm^{-1} for **1** and 1648 cm^{-1} for **2** thus, indicating the coordination of the azomethine nitrogen to Pd(II) ion,[22–24] which is further confirmed by the appearance of a band at 425–430 cm^{-1} assigned to a ν_{Pd-N} vibration.[25] The stretching band observed at *ca*. 3270 cm^{-1} due to the ν_{Ph-OH} group in the free ligand disappears in Pd(II) complexes due to deprotonation. A band which appeared at 1278 cm^{-1} (phenolic C–O) in the free ligand has been shifted to higher frequency and

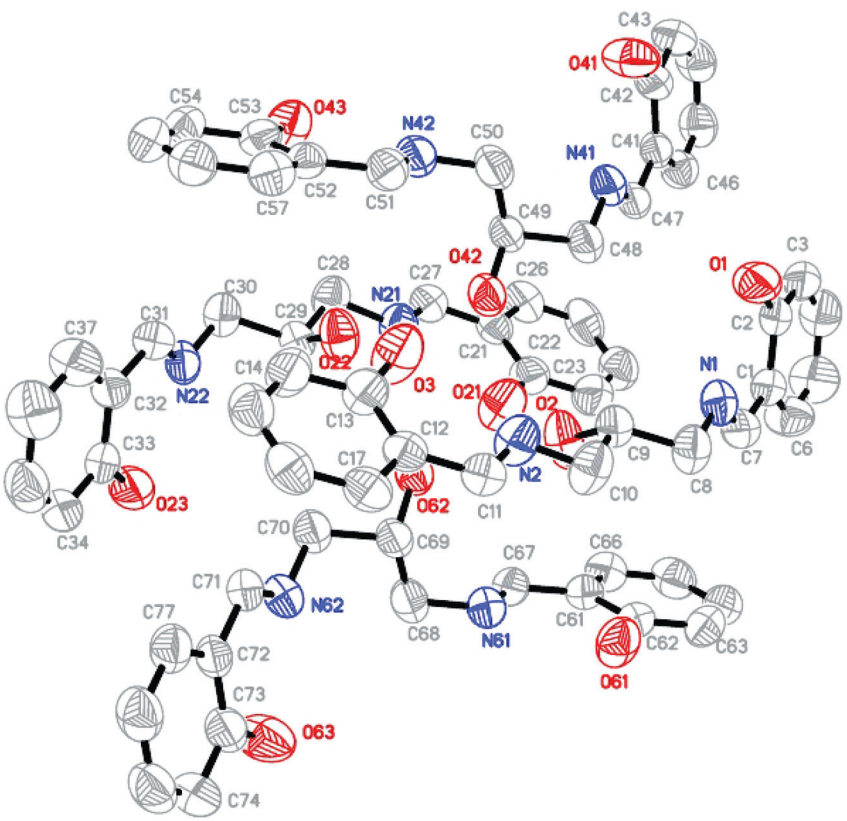

Fig. 1 ORTEP diagram of free ligand **L** plotted with 50% probability of displacement ellipsoids. Some atom labels and hydrogen atoms are omitted for clarity.

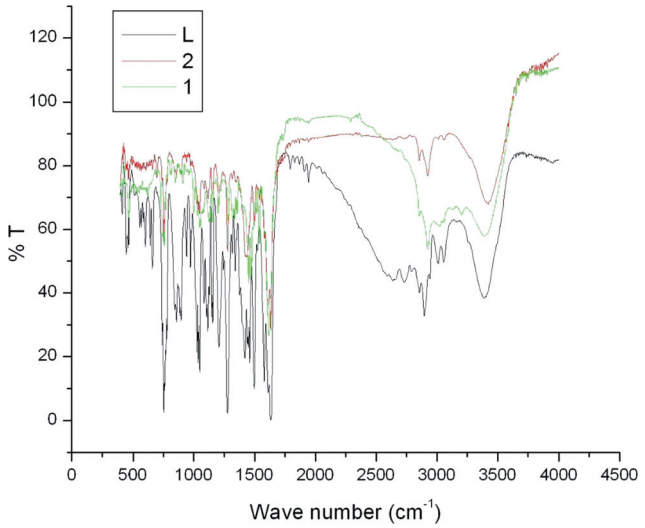

Fig. 2 IR Spectra of free ligand **L** and complexes **1** and **2**.

appears at 1290 and 1282 cm^{-1} in **1** and **2**, respectively, suggesting coordination through the phenolic oxygen atom.[24] The absorption band corresponding to the –OH group of diaminopropanol remains unchanged in the Pd(II) complexes revealing that the –OH group of the diaminopropanol does not take part in coordination.[26] The absorption band appearing at 295 cm^{-1} in **1** is assigned to ν_{Pd-Cl}, while **2** shows two absorption bands at 1637 and 1430 cm^{-1}, assignable to $\nu_{a\ COO}$ and $\nu_{s\ COO}$ stretching vibrations of the carboxylate group, respectively, indicating the monodentate coordination of the acetate group to the Pd(II) ion.[27]

3.3 ^{1}H and ^{13}C NMR spectroscopic analyses

The ^{1}H NMR spectrum of the free ligand exhibits a singlet at 13.82 ppm assigned to the aromatic-OH proton, which is absent in the Pd(II) complexes indicating the coordination of phenolic oxygen to the Pd(II) ion. A azomethine proton due to –CH═N was observed at 8.35 ppm, which upon coordination to Pd(II) ion showed a downfield shift and occurred at 8.41 and 8.56 ppm for **1** and **2**, respectively (Fig. 3, Fig. 1S, ESI†). The ^{1}H NMR spectrum of ligand **L** also shows a series of multiplets due to aromatic protons in the 6.79–7.10 ppm range. As expected, upon coordination to Pd(II) ion, these signals show small shifts due to the ligand electronic redistribution attributed due to interaction of the ligand with the Pd(II) ion. In addition, chemical shifts for –CH (s, 1H) and $-CH_2$ (d, 4H) protons in the free ligand appear at 3.65 and 3.58–3.65 ppm, respectively. ^{1}H NMR spectra are further supported by ^{13}C NMR spectra results (Fig. 4, Fig. 2S, ESI†). The ^{13}C NMR spectrum of the salen ligand shows a number of signals corresponding to the various carbon atoms expected due to their non-equivalence. Free ligand **L** shows a sharp signal corresponding to the azomethine carbon at 163.68 ppm while the signals for $-CH_2$ and –CH carbons appear at 62.85 and 69.15 ppm, respectively. The ^{13}C NMR signals for aromatic carbons appear at 160.15, 131.85, 131.91, 116.45, 118.50 and 117.21 ppm. These values undergo a downfield shift upon coordination to Pd(II) ion. Complex **2** shows a sharp signal

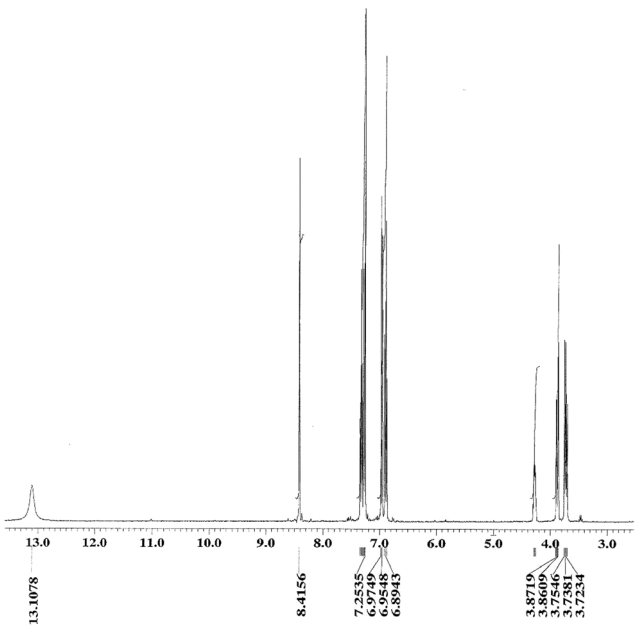

Fig. 3 ^{1}H NMR spectrum of complex **1**.

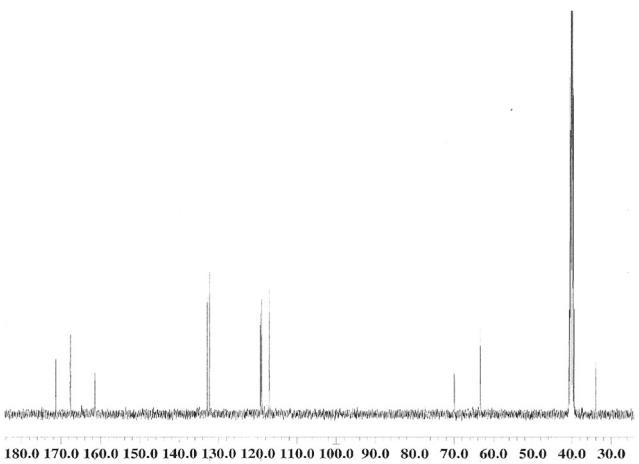

Fig. 4 ^{13}C NMR spectrum of complex **2**.

at 172.25 ppm attributed to the –CH═N carbon while the signals for $-CH_2$ and –CH carbons appear at 63.85, 70.15 ppm. The signals for aromatic carbons appear at 160.75, 161.80, 132.15, 132.25, 117.75 and 118.23 ppm (Fig. 4). Similarly, a sharp signal for the azomethine carbon appears at 167.57 ppm in complex **1**. The signals for $-CH_2$ and –CH carbons appear at 63.36 and 70.58 ppm, respectively, while the signals for the aromatic carbons appear at 161.03, 132.71, 131.68, 118.92, 118.72 and 117.07 (Fig. 2S, ESI†).

3.4 Mass spectrometry

The structure of the complexes was also supported by mass spectrometry under positive-ion ESI condition. The ESI-MS spectra of the synthesized ligand and its Pd(II) complexes show the presence of the molecular ion as its sodium adduct $[M + Na]^{+}$. The

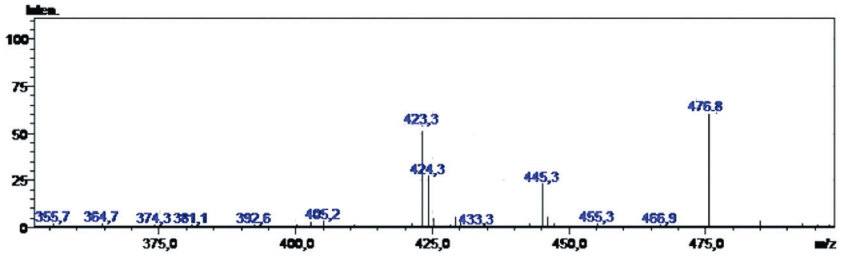

Fig. 5 ESI-MS spectrum of complex **1**.

ESI-MS spectra showed molecular ion peaks $[M + Na]^+$, *m/z* at 299.34, 476.67, 522.84 corresponding to their molecular formulae, **L**, $[PdLCl_2]$ and $[PdL(OAc)_2]$, with the corresponding calculated *m/z* being 298.34, 475.67, 522.85, respectively (Fig. 5).

3.5 UV-Vis studies

The UV-Vis absorption spectra of the Pd(II) complexes have been recorded in the 200–800 nm range in dichloromethane (Fig. 6). The bands below 321 nm are attributed to π–π* and n–π* transitions of the ligands.[28,29] All Pd(II) complexes are diamagnetic with a square-planar geometry, for which three spin-allowed d–d transitions are expected, corresponding to transitions from the three lower lying d-levels to the empty $d_{x^2-y^2}$ orbitals.[30] The most prominent absorption bands appear at 401 and 397 nm for **1** and **2**, respectively, ascribed to the metal-to ligand charge transfer transitions.[28,29]

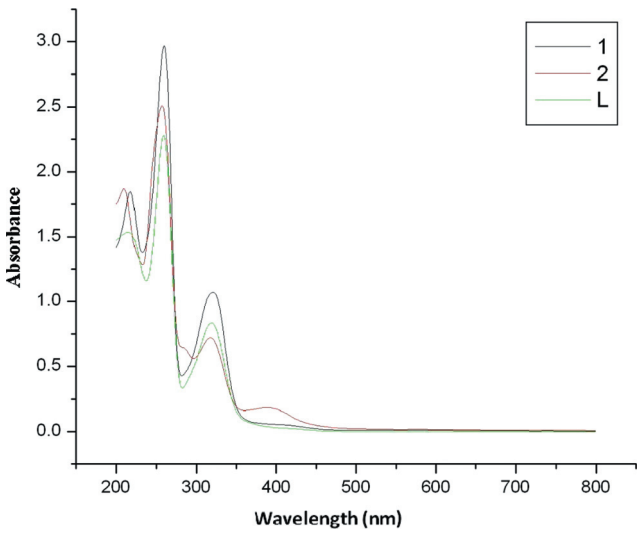

Fig. 6 UV-Vis spectra of ligand **L** and complexes **1** and **2**.

3.6 Thermogravimetric analyses

Thermal stabilities of **1** and **2** were carried out by thermogravimetric analyses (TGA and DTA) in N_2 atmosphere at a heating rate of 20 °C min^{-1} in the temperature range 20–800 °C. These compounds undergo three steps of weight loss (Fig. 7). The TGA of **2** shows a first weight loss of 11.45% corresponding to coordinated water and acetate ion in the temperature range of 30–252 °C. Further elevation in temperature from 252–485 °C leads to a rapid weight loss of *ca.* 48.55% attributed to dissociation of the salen ligand at the imine bond. A gradual weight loss in the temperature range 485–800 °C leads to the complete decomposition of the organic moiety leaving a final residue of PdO. The total weight loss up to 800 °C is found to be 60%. The TGA data is further supported by DTA, which shows three main steps at 20–200, 200–452 and 452–800 °C. The maximum weight loss of *ca.* 14% min^{-1} occurred in the second stage at 200–452 °C. The results of TGA and DTA clearly indicated that the second stage is the main degradation stage.

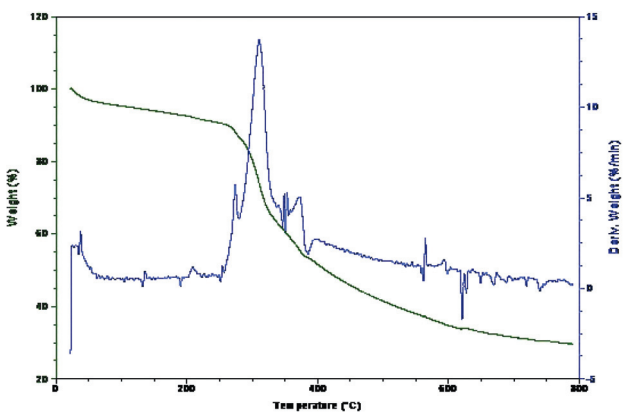

Fig. 7 TGA/DTA curve of complex **1**.

3.7 DNA binding studies

UV-Vis absorption studies were performed to further ascertain the interaction of ligand and its Pd(II) complexes with DNA. The UV absorbance showed an increase in absorbance at 260 nm with increasing concentrations of free ligand **L** and complexes **1** and **2** (Fig. 8). The rise in the DNA absorbance is indicative of the interaction between DNA and the synthesized compounds. The obtained results showed that free ligand **L** and its complexes exhibited hyperchromism (increase in absorbance) but of varied degree. Complexes **1** and **2** showed greater affinity for DNA as compared to free ligand **L**. Interestingly, both the complexes, **1** and **2** showed approximately equal binding strength with DNA. Hypochromism and hyperchromism are both spectral features of DNA connected with its double helix structure. Hypochromism means the DNA-binding mode of the complex is electrostatic or intercalative which can stabilize the DNA duplex.[31,32] Contrary

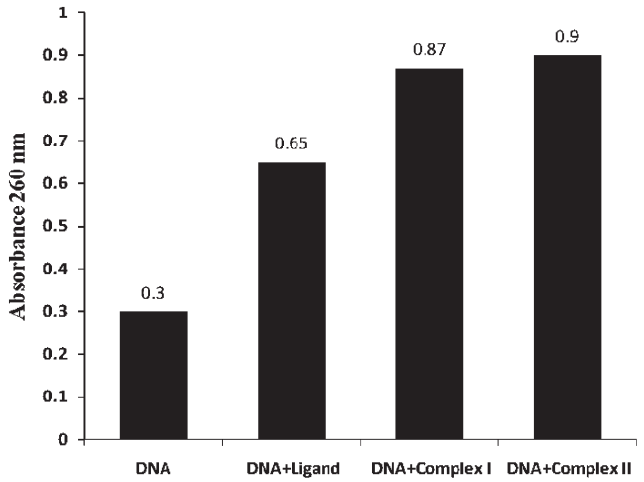

Fig. 8 Absorbance spectroscopy of DNA at 260 nm with ligands and its complexes: DNA concentration = 0.1 mM and concentration of ligand and the complexes = 50 μM.

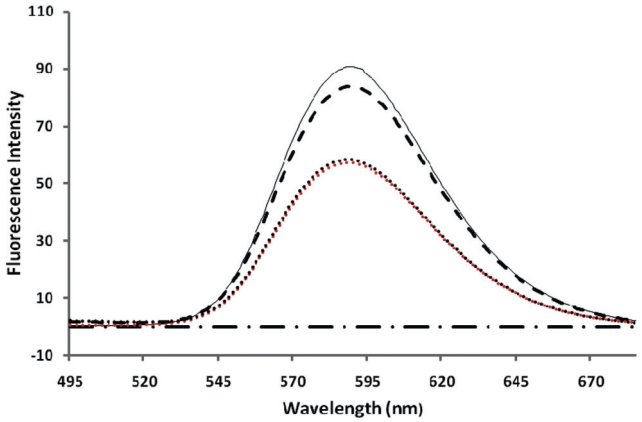

Fig. 9 Fluorescence emission spectra of ethidium bromide (EB) bound to DNA in the absence and presence of ligand and complex: EB alone (-··-); EB + DNA (—); EB + DNA + ligand (---); EB + DNA + complex **1** (···), EB + DNA + complex **2** (■ ■ ■).

to this, hyperchromism indicates the breakage of the secondary structure of DNA. So we speculate that our synthesized compounds (free ligand **L** and its Pd(II) complexes **1** and **2**) interact with the secondary structure of calf thymus DNA resulting in its breakage and perturbation.

Further, ethidium bromide displacement assay for DNA binding study with free ligand **L** and complexes **1** and **2** were studied using fluorescence spectroscopy. Nucleic acid bound to some molecules generally exhibits marked changes in fluorescence properties and this phenomenon is used in studies with DNA.[33] Ethidium bromide, a polycyclic aromatic dye, is the most widely used fluorescence probe for DNA structure. EB displays very weak fluorescence in aqueous solution. However, in the presence of DNA, it exhibits intense fluorescence because of intercalation with base pairs in DNA.[34] Our results showed that the addition of free ligand **L** and complexes **1** and **2** to DNA complexed with EB causes appreciable reduction in emission intensity, indicating that synthesized compounds show competitive binding with EB for DNA and thus reaffirm the binding of these novel synthesized molecules with DNA. Moreover, results showed complexes **1** and **2** had a greater quenching effect as compared to free ligand **L**, thus indicating greater affinity of both the complexes when compared to the free ligand. On the basis of the above results, we suggest that free ligand **L** and complexes **1** and **2** have the ability to interact with DNA. In contrast with the UV-vis absorption studies above, the affinity for DNA is seen to be higher for complex **1** when compared with complex **2** (and free ligand **L**), as suggested by the higher K_{SV} for complex **1** in comparison to complex **2** and free ligand **L**. This difference in the DNA binding ability could be due to the presence of an electron deficient center in the charged Pd(II) complex where an additional interaction between the complex and phosphate rich DNA backbone may occur.[35] It has been reported that the enhanced fluorescence of the EB–DNA complex can be quenched at least partially by the addition of a second molecule and this could be used to assess the relative affinity of the molecule for DNA (Fig. 9).[36]

3.8 Effect of free ligand L and of complexes 1 and 2 on cell proliferation

To test *in vitro* anti-proliferative effect of synthesized compounds (free ligand **L**, complexes **1** and **2**) on hepatocellular carcinoma cell lines (Huh7), the treatment dose was optimized to avoid cell cytotoxicity. Huh7 cells were seeded at the same density and subjected to the optimum dose of these compounds along with control (CTL) in six well plates. The optimized dose was used to treat at 0 h and the anti-proliferative effect was analyzed at different times of 0, 12, 24 and 48 h. As shown in Fig. 1, the number of cells at 12 h of treatment was significantly less in complexes **1** and **2** treated wells. The effect of free ligand **L** at 12 h of treatment was similar to that of the control. At 24 and 48 h, the cells treated with complexes **1** and **2** showed significant anti-proliferative effects compared to free ligand **L** and control (Fig. 10a, b). Complexes **1** and **2** significantly reduce the cell doubling time as well showing limited cytotoxicity. Thus, our anti-proliferative data confirmed the role of complexes **1** and **2** in reducing the cell doubling time and hence proliferation.

3.9 Effect of free ligand L and of complexes 1 and 2 on tumor promoting genes

The cells treated with optimized concentration of free ligand **L** and of complexes **1** and **2** along with vehicle control alone were subjected to total cellular RNA isolation. The total cellular RNA was collected and analyzed for the expression of Wnt-1 and uPA mRNA levels. Our data indicate that Huh7 cells treated with complexes **1** and **2** significantly reduce the expression of Wnt-1 mRNA levels (Fig. 11a). The reduction was not significantly observed in ligand **L** alone treated Huh7 cells compared to the control. Similar effects were not observed with the level of urokinase plasminogen activator (uPA) mRNA, when cells were treated with free ligand **L**, complexes **1** and **2**; as shown in Fig. 11b, uPA levels were all similar to that of the vehicle control. Our result demonstrated that complexes **1** and **2** reduce

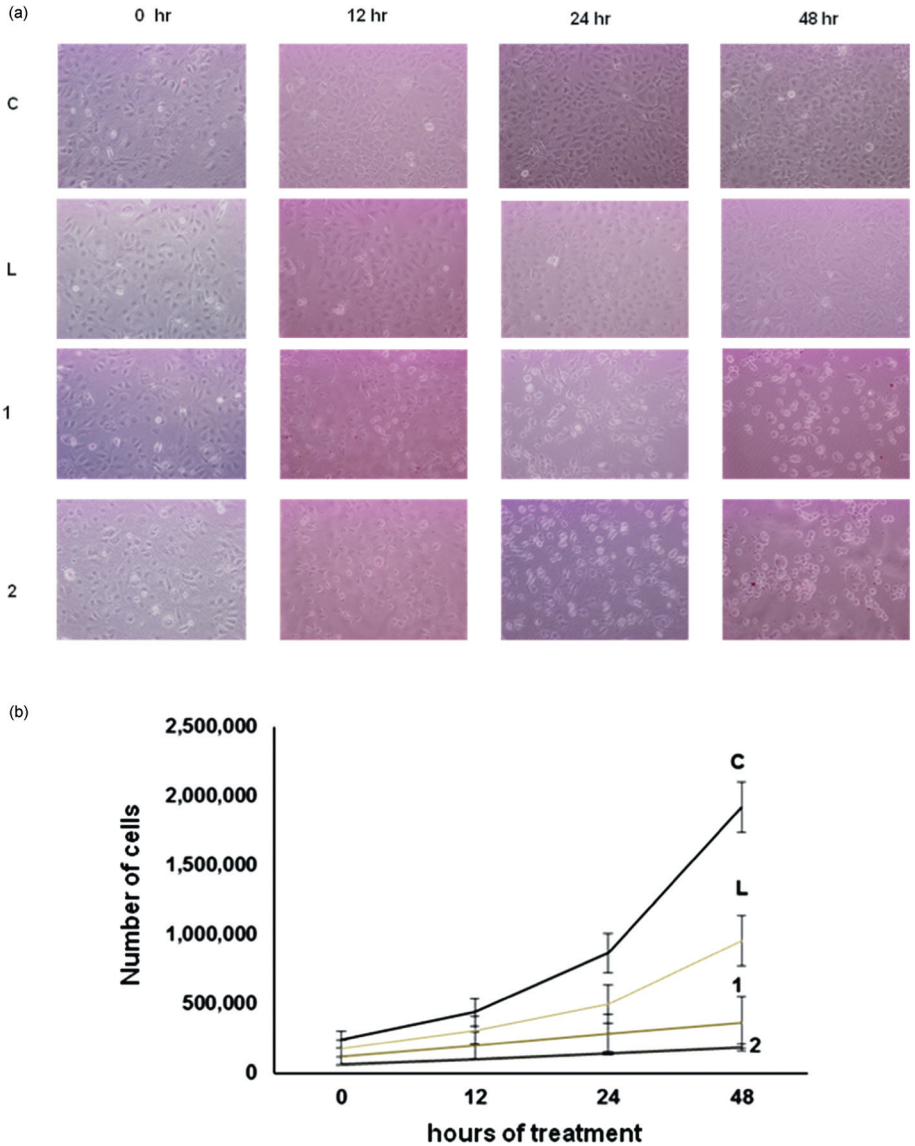

Fig. 10 Effect of ligand **L** alone and of complexes **1** and **2** on the proliferation of Huh7 cells. Huh7 cells were seeded at the same density a day before treatment. Next day the cells were subjected to treatment with an optimized concentration of **L** alone, complexes **1** and **2**, or vehicle control alone (DMSO) in a six well plate. The anti-proliferative effect of these compounds was measured microscopically at different time intervals and also by growth curve analysis. At each time point (12, 24 and 48 h), cells were trypsinized and counted as described in the Materials and methods section. All data presented are expressed as mean ± SEM of triplicate wells for each time point. Significant difference from the control is represented by an asterisk ($P < 0.05$).

the tumor promoting gene Wnt-1 but not the prometastatic gene uPA.

3.10. Effect of free ligand L, 1 and 2 on tumor suppressor gene (RASSF1A)

The tumor suppressor gene (RASSF1A) has been studied in several cancers, and it has been reported that a large number of patients have inactivated RASSF1, while a similar number have a tumor in which the RASSF1A pathway is partially abrogated by inactivation of other signaling components. Since, it influences a large number of proteins, the effect of compounds on the mRNA expression of RASSF1A have been investigated. Total cellular RNA (treated and control) was analyzed for the expression of RASSF1A. Our results show that complexes **1** and **2** treated Huh7 cells significantly enhance the RASSF1A mRNA level compared to control group (Fig. 11c). This effect was not observed in free ligand **L** treated cells, and the mRNA expression level was very similar to that of the control (Fig. 11c).

3.11 Effect of free ligand L, 1 and 2 on transforming growth factor-β (TGF-β)

Transforming growth factor-beta (TGF-β) is a multifunctional cytokine involved in the regulation of growth and differentiation

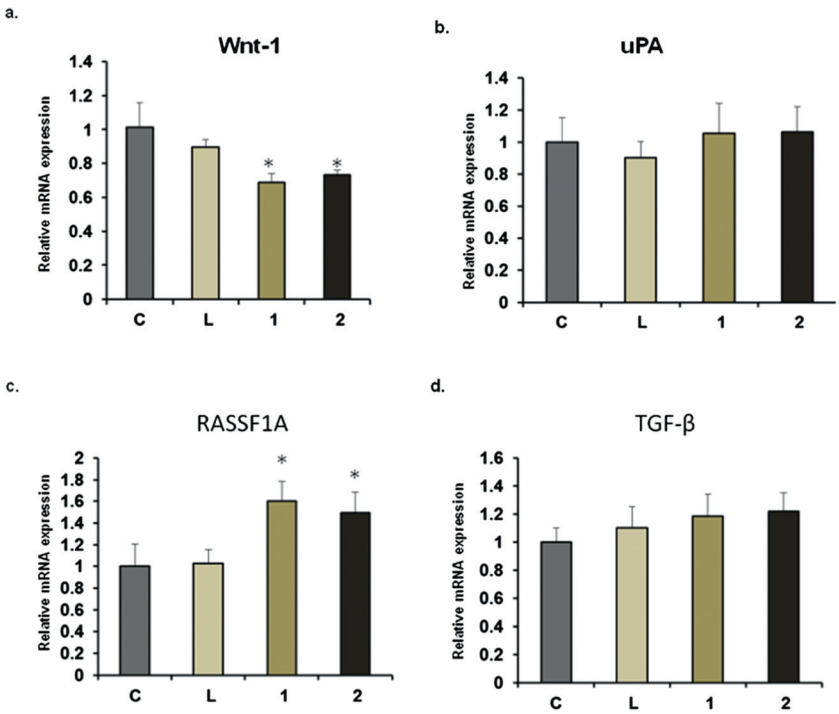

Fig. 11 Effect of ligand **L** alone and complexes **1** and **2** on the expression of tumor promoting and suppressor genes. Huh7 cells were treated with ligand **L** alone or complexes **1** and **2** and at the end of experiment, total cellular RNA was isolated with Trizol. RNA from control and treatment groups were analyzed for the expression of genes (10a) Wnt, (10b) uPA, (10c) RASSF1A and (10d) TGF-β by real time PCR. Changes in the mRNA expression of the respective genes were determined as relative mRNA expression against internal control GAPDH. Experiments were repeated three times and significant differences from the control are represented by an asterisk ($P < 0.05$).

of both normal and transformed cells. Therefore, we have investigated how these compounds effect the mRNA expression in hepatocellular carcinoma cell line. We found that all of our synthetic compounds insignificantly enhanced the mRNA expression of TGF-β (Fig. 11d).

Free ligand **L** and its complexes **1** and **2** were tested for *in vitro* antitumor and anti-proliferative activity and expression of different genes involved in cancer. On the basis of our experimental results, complexes **1** and **2** showed a strong dose dependent growth inhibition of Huh7 cells compared to DMSO (control) treated cells. The free ligand **L** exhibits a much reduced inhibitory effect compared to complexes **1** and **2**. The anti-proliferative effect of complexes **1** and **2** corroborate earlier findings of palladium complex derivatives that demonstrate a strong dose dependent growth inhibition.[37,38] To determine whether these compounds effect key players in cancer, we measured the level of expression of Wnt-1, uPA, RASSF1 and TGF-β by real-time PCR. In mammals, Wnt signaling is complex and regulates diverse functions including initiation and progression of cancer.[39–42] Therefore, we have tested the effect of our synthetic compounds on the mRNA expression of Wnt-1. Complexes **1** and **2** demonstrated significant inhibition of Wnt-1 expression compared to DMSO treated control. The free ligand **L** treated cells showed decreased Wnt-1 mRNA expression but this was not nearly as significant as for complexes **1** and **2**. These findings establish that the Pd(II) complexes have anti-proliferative and anticancer effects compared to the parent ligand. Another important gene (uPA) analyzed in our study is involved in the metastatic cascade and implicates the degradation of the extracellular matrix and subsequent invasion by cancer cells.[43–45] Due the importance of this gene in metastasis, we analyzed its mRNA expression in the presence of the synthetic compounds. Surprisingly, none of the compounds suppress or activate the expression of uPA mRNA in the Huh7 cell line. In most of cancers, uPA is epigenetically regulated as the promoter region of this gene is hypomethylated.[46] The level of uPA mRNA expression is regulated by the methylation pattern (epigenome), and may be a reason why these compounds had no effect on the expression of mRNA.

The Ras-association domain family 1A (RASSF1A) gene is a new candidate tumor suppressor gene (TSG) and has been reported to play an important role in the malignant progression of many tumors.[47–49] Due to its role in development of HCC, we have tested the expression of this gene in the presence of our compounds. The finding was remarkable and showed enhanced RASSF1A expression in the presence of complexes **1** and **2**, although free ligand **L** expression was similar to the control group. We speculate that complexes **1** and **2** may be involved in genetic alternations and hence gain in RASSF1A expression. How these compounds alter the genetic structure needs to be analyzed in detail. Transforming growth factor-β (TGF-β) is a pleiotropic cytokine that regulates cell proliferation, angiogenesis, metastasis and immune suppression.[50,51] TGF-β has a biphasic effect in tumor growth; carcinogenesis and early tumor growth are suppressed by TGF-β whereas this growth factor apparently accelerates tumor progression in more advanced

aggressive tumors.[49,50] Therefore, the effect of these compounds on the mRNA expression has been investigated. There was insignificant increase in the level of mRNA expression compared to the control when Huh7 cells were treated with free ligand **L** and complexes **1** and **2**.

4. Conclusion

A series of novel mononuclear Pd(II) complexes derived from a salen ligand has been synthesized and characterized by elemental analyses and various spectroscopic studies. UV/Vis data reveal a square-planar geometry around the Pd(II) ion in the complexes. The structure of ligand has been confirmed by single-crystal XRD. The ligand and its complexes have been tested against a human hepatoma cancer cell line and results suggest that Pd(II) complexes have significant anti-proliferative effects.

Acknowledgements

This work is supported by Research Centre, College of Science, King Saud University, Riyadh KSA.

References

1 N. J. Wheate, S. Walker, G. E. Craig and R. Oun, *Dalton Trans.*, 2010, **39**, 8113–8127.
2 A. G. Quiroga, F. J. Ramos-Lima, A. Alvarez-Valdés, M. Font-Bardía, A. Bergamo, G. Sava and C. Navarro-Ranninger, *Polyhedron*, 2011, **30**, 1646–1650.
3 S. J. Lippard and P. Pil, *Encyclopedia of Cancer, Cis-Platin and Related Drugs*, Academic Press, San Diego, CA, 1997, 392–410.
4 F. J. Ramos-Lima, A. G. Quiroga and J. M. Perez, Carmen Navarro-Ranninger, *Polyhedron*, 2003, **22**, 3379–3381.
5 *Cisplatin*, ed. B. Lippert, Verlag Helvetica Chim Acta, Postfact, CH-8042, Zürich, Switzerland, 2006.
6 S. van Zutphen and J. Reedjik, *Coord. Chem. Rev.*, 2005, **249**, 2845–2853.
7 M. J. Clarke, F. Zhu and D. R. Frasca, *Chem. Rev.*, 1999, **99**, 2511.
8 T. Schilling, B. K. Keppler and M. E. Heim, *Invest. New Drugs*, 1995, **13**, 327.
9 A. S. Abu-Surrah and M. Kettunen, *Curr. Med. Chem.*, 2006, **13**, 1337–1357.
10 G. Zhao and H. Lin, *Curr. Med. Chem.: Anti-Cancer Agents*, 2005, **5**, 137–147.
11 D. Kovala-Demertzi, A. Bocarelli, M. A. Demertzis and M. Coluccia, *Chemotherapy*, 2007, **53**, 148–152.
12 N. J. Wheate, S. Walker, G. E. Craig and R. Oun, *Dalton Trans.*, 2010, **39**, 8113–8127.
13 E. C. Niederhoffer, J. H. Timmons and A. E. Martell, *Chem. Rev.*, 1984, **84**, 137.
14 K. Srinivasan, P. Michaud and J. K. Kochi, *J. Am. Chem. Soc.*, 1986, **108**, 2309.
15 W. Zhang, J. L. Loebach, S. R. Wilson and E. N. Jacobsen, *J. Am. Chem. Soc.*, 1990, **112**, 2801.
16 J. Tisato, F. Refosco and F. Bandoli, *Coord. Chem. Rev.*, 1994, **135–136**, 325.
17 J. Fonseca, J. Martinez, L. C. Silva, A. L. Magalhães, M. T. Duarte and C. Freire, *Inorg. Chim. Acta*, 2010, **363**, 4096–4107.
18 *X-RED. Version 1.18*, STOE & Cie GmbH, Darmstadt, Germany, 1999.
19 G. M. Sheldrick, A short history of SHELX, *Acta Crystallogr., Sect. A: Found. Crystallogr.*, 2007, **64**, 112–122.
20 A. M. Pyle, J. P. Rehmann, R. Meshoyrer, C. V. Kumar, N. J. Turro and J. K. Barton, *J. Am. Chem. Soc.*, 1989, **111**, 3051–3058.
21 G. R. Desiraju and T. Steiner, *The Weak Hydrogen Bond in Structural Chemistry and Biology*, Oxford University Press, Oxford, 1999.
22 L. J. Baucher, *J. Inorg. Nucl. Chem.*, 1974, **36**, 531–536.
23 J. Uttamachandani and R. N. Kapoor, *Transition Met. Chem.*, 1978, **3**, 79–81.
24 N. Dharmaraj, P. Viswanathamurthi and K. Natarajan, *Transition Met. Chem.*, 2001, **26**, 105–109.
25 K. I. Goldberg, J. V. Martinez, G. E. Perez, L. J. Ackerman and D. X. West, *Polyhedron*, 1999, **18**, 1177–1182.
26 L. D. Popov, Y. P. Tupolova, V. V. Lukov, I. N. Shcherbakov, A. S. Burlov, S. I. Levchenkov, V. A. Kogan, K. A. Lyssenko and E. V. Ivannikova, *Inorg. Chim. Acta*, 2009, **362**, 1673–1680.
27 K. Nakamoto, *Infrared and Raman Spectra of Inorganic and Coordination Compounds*, Wiley, New York, 1986, Mir, Moscow 1991.
28 A. B. P. Lever, *Inorganic Electronic Spectroscopy*, Elsevier, New York, 2nd edn, 1984.
29 M. Ulusoy, O. Birel, O. Sahin, O. Buyukgungor and B. Cetinkya, *Polyhedron*, 2012, **38**, 141–148.
30 H. H. Jaffe and M. Orchin, *Theory and Applications of Ultraviolet Spectroscopy*, J. Wiley, New York, 1962.
31 E. C. Long and J. K. Barton, *Acc. Chem. Res.*, 1990, **23**, 271.
32 R. Sujata, S. Rona and S. Munna, *J. Inorg. Biochem.*, 2006, **100**, 1320.
33 C. Liu and J. Zhou, *J. Inorg. Biochem.*, 1998, **71**, 1–6.
34 F. Leng, D. Graves and J. B. Chaires, *Biochim. Biophys. Acta, Gene Struct. Expression*, 1998, **1442**, 71–81.
35 J. Liu, T. Zhang, T. Lu, L. Qu, H. Zhou, Q. Zhang and L. Ji, *J. Inorg. Biochem.*, 2002, **91**, 269–276.
36 S. Yellappa, J. Seetharamappa, L. M. Rogers, R. Chitta, R. P. Singhal and F. D'Souza, *Bioconjugate Chem.*, 2006, **17**, 1418–1425.
37 L. Giovagnini, L. Ronconi, D. Aldinucci, D. Lorenzon, S. Sitran and D. Fregona, *J. Med. Chem.*, 2005, **48**, 1588–1595.
38 H. Cheng, F. Huq, P. Beale and K. Fisher, *Eur. J. Med. Chem.*, 2006, **41**, 896–903.
39 W. Wei, M.S. Chua and S. Grepper, *Mol. Cancer*, 2009, **8**, 76.
40 Y. Takigawa and A. M. Brown, *Curr. Drug Targets*, 2008, **9**, 1013–1024.
41 S. B. Nambotin, J. R. Wands and M. Kim, *Anti-Cancer Agents Med. Chem.*, 2011, **11**, 549–559.
42 H. C. Lee, M. Kim and J. R. Wands, *Front. Biosci.*, 2006, **11**, 1901–1915.
43 P. A. Andreasen, L. Kjoller, L. Christensen and M. J. Duffy, *Int. J. Cancer*, 1997, **72**, 1–22.
44 S. A. Rabbani, *In Vivo*, 1998, **12**, 135–142.
45 S. A. Rabbani and A. P. Manzar, *Surg. Oncol. Clin. N. Am.*, 2001, **10**, 393–415.
46 N. Shukeir, P. Pakneshan, G. Chen, M. Szyf and S. A. Rabbani, *Cancer Res.*, 2006, **66**, 9202–9210.
47 R. Dammann, C. Li, J. H. Yoon, P. L. Chin, S. Bates and G. P. Pfeifer, *Nat. Genet.*, 2000, **25**, 315–19.
48 K. Dreijerink, E. Braga and I. Kuzmin, *Proc. Natl. Acad. Sci. U. S. A.*, 2001, **98**, 7504–7509.
49 L. Shivakumar, J. Minn, T. Sakamaki, R. Pestell and M. A. White, *Mol. Cell. Biol.*, 2002, **22**, 4309–4318.
50 A. Nawshad, D. Lagamba, A. Polad and E. D. Hay, *Cells Tissues Organs*, 2005, **179**, 11–23.
51 R. L. Elliott and G. C. Blobe, *J. Clin. Oncol.*, 2005, **23**, 2078–2093.